

## WHEAT IMPURITY DETECTION ALGORITHM BASED ON IMPROVED YOLO v8

## / 基于改进 YOLO v8 的小麦杂质检测算法

Liqing ZHAO, Rui QIAN, Chuang LIU, Shuhao WANG, Junjie XIA

College of Electrical and Mechanical Engineering, Qingdao Agriculture University, Qingdao / China;

Tel: +86-13222725599; E-mail: [758128332@qq.com](mailto:758128332@qq.com)DOI: <https://doi.org/10.35633/inmateh-75-62>**Keywords:** Wheat Impurity Detection, YOLOv8, Multi-scale Feature Fusion, Lightweight Design**ABSTRACT**

To achieve fast and accurate detection of wheat impurities, this study proposes an improved YOLOv8-based algorithm that targets three typical impurity types: bran, straw, and spike. The original C2f module is replaced with the C2f\_UIB structure from MobileNetV4 to reduce model complexity, and a High-level Screening Feature Pyramid Network (HS-FPN) is integrated to enhance multi-scale feature fusion. Additionally, a Generalized IoU loss function is adopted to improve detection robustness in dense impurity scenarios. The optimized model is deployed on an embedded Jetson Nano platform for real-time inference, coupled with an industrial camera and LED lighting system. To validate its practical effectiveness, an indoor experimental setup was constructed to simulate field conditions. A total of 30 wheat samples were tested, and results demonstrate high consistency between system detection and manual annotation, with minimal deviation across all impurity types. The proposed algorithm exhibits excellent accuracy, lightweight characteristics, and strong potential for deployment in intelligent agricultural equipment.

**摘要**

为实现对小麦杂质的快速准确检测, 本文提出一种基于改进 YOLOv8 的杂质识别算法, 主要针对三类典型杂质: 麦麸、秸秆和麦穗。该算法将 YOLOv8 中的 C2f 模块替换为 MobileNetV4 的 C2f\_UIB 结构, 以降低模型复杂度, 并引入高级筛选特征金字塔网络 (HS-FPN) 以提升多尺度特征融合能力。此外, 采用广义 IoU 损失函数以增强高密度杂质场景下的检测鲁棒性。优化后的模型部署于 Jetson Nano 嵌入式平台, 并结合工业相机与 LED 面光源构建图像采集系统, 实现了模型的实时推理。为验证其实际应用效果, 搭建室内试验平台模拟田间作业环境, 对 30 组小麦样本进行了检测实验。结果显示, 系统识别结果与人工标注高度一致, 各类杂质检测误差极小, 表明所提算法具备良好的检测精度、轻量化特性及农业装备部署应用潜力。

**INTRODUCTION**

Wheat is one of the most important staple crops globally, playing a critical role in food security and economic development. However, the presence of impurities such as straw, wheat bran, and other foreign materials during the harvesting process significantly affects the quality and market value of wheat. Traditional methods for impurity detection rely heavily on manual labor, which is not only time-consuming but also prone to human error. With the aging agricultural workforce and rising labor costs, there is an urgent need for automated and precise impurity detection systems to improve the efficiency and quality of wheat harvesting.

In early research on visual impurity detection in agriculture, traditional image processing techniques such as color thresholding and morphological filtering were commonly used.

Chen *et al.* (2020) proposed a machine vision-based real-time impurity detection system for rice combine harvesters, employing decision tree algorithms to classify grain morphological features (A1-A6). The integrated lateral illumination system and decision tree model achieved 76% classification accuracy on training datasets, establishing a foundation for real-time parameter optimization in harvesting machinery.

Marjanović *et al.* (2018) developed a rainfall-triggered landslide prediction model using decision tree algorithms to analyze precipitation data from 2001-2014. Critical thresholds of 30 mm rainfall in 2-3 days and 140 mm cumulative rainfall over 30 days were identified, revealing dominant mechanisms of medium-term rainfall impacts on landslides in Western Serbia.

Ok *et al.* (2012) applied random forest with parcel-based analysis to SPOT5 imagery crop classification, achieving 85.89% overall accuracy (8% improvement over maximum likelihood methods), demonstrating superiority in multispectral interpretation.

*Mavridou et al. (2019)* systematically reviewed agricultural machine vision technologies across seven domains (fruit grading/yield estimation/disease detection), analyzing multi-sensor integration strategies to guide precision agriculture implementation.

These traditional methods are limited by their reliance on handcrafted features, low adaptability to complex environments, and difficulty in handling high-density impurity scenarios. In contrast, deep learning techniques have shown great potential by leveraging convolutional neural networks (CNNs) to automatically extract multi-level semantic features.

Deep learning overcomes these limitations by leveraging convolutional neural networks (CNNs) to automatically extract multi-level features.

*Shen and Zhao (2021)* proposed a lightweight YOLOv3-based detection model for peanut sorting systems, solving missed detection problems while ensuring real-time inference on CPUs.

*Qi et al. (2023)* designed a GhostNet-based pest detection model with attention-guided receptive field fusion, achieving high mAP and FPS under lightweight constraints.

*Shi et al. (2023)* developed a DCGA-YOLOv8 system for multi-crop navigation line extraction, achieving 98.9%-100% correct clustering rates for cabbage/kohlrabi/rice. The integration of threshold-optimized DBSCAN and B-spline curve modelling enabled safe agricultural machinery path planning.

*Jia et al. (2024)* proposed ADL-YOLOv8 for weed detection, incorporating AKConv networks and DySample upsampling. The model improved mAP@0.5 by 3.07% while maintaining 15.77% compression rate, providing lightweight high-precision solutions for smart weeding devices.

*Zhang et al. (2024)* built HR-YOLOv8 for crop growth monitoring using dual self-attention mechanisms and parallel feature fusion. The model enhanced detection accuracy by 5.2% for oil palm and 0.6% for strawberries, enabling high-resolution feature preservation.

*Jiang et al. (2022)* optimized YOLOv7 with CBAM attention modules for Muscovy duck flock counting, achieving 98.6% accuracy and 2.3% mAP@0.5 improvement over baseline models, supporting automated density monitoring in poultry farming.

*Wang et al. (2022)* streamlined YOLOv5s for real-time apple calyx/stem recognition via detection head search and channel pruning. The compressed model achieved 25.51 FPS on CPUs with 93.89% accuracy, enabling efficient automated sorting.

*Mathew and Mahesh (2022)* deployed YOLOv5 for bell pepper bacterial spot detection, implementing whole-image feature extraction to identify micro-lesions, providing early disease warnings for mobile agricultural systems.

These studies highlight that deep learning not only supports real-time multi-target recognition in complex scenes, but also enables flexible model design through end-to-end training.

In the domain of wheat impurity detection, several notable deep learning-based methods have emerged recently.

*Zhou et al. (2023)* proposed WheNet, an Inception-v3-based CNN that achieved 98.59% Top-1 accuracy for classifying wheat and five impurity types.

*Li et al. (2023)* combined terahertz 3D imaging with a metaheuristic RetinaNet model (AHA-RetinaNet-X), obtaining over 95% accuracy for impurity classification in non-destructive testing.

*Chen et al. (2022)* developed Ro-YOLOv5 based on rotated bounding boxes and Circular Smooth Labels, significantly improving impurity detection in wheat CT images.

However, many of these approaches rely on complex imaging systems (e.g., THz, CT), large-scale models, or lack the ability to run in real-time on resource-limited embedded devices. In addition, some methods focus on image classification rather than instance-level detection and localization, which limits their deployment in actual harvesting scenarios.

To address these challenges, this study proposes a lightweight wheat impurity detection algorithm based on an improved YOLOv8 architecture, integrating a Universal Inverted Bottleneck (UIB) module for computational efficiency, a High-level Screening Feature Pyramid Network (HS-FPN) for multi-scale fusion, and a GloU-based loss function for robust object localization. The model is deployed on a Jetson Nano embedded platform with industrial camera input, and validated through indoor experiments simulating real-world conditions. Compared with existing methods, our approach achieves high accuracy, fast inference, and low computational cost, making it highly suitable for intelligent agricultural equipment in modern farming environments.

## MATERIALS AND METHODS

The wheat used in this study was provided by the Xizhai Agricultural Machinery Cooperative in Tianzhuang Town, Pingdu City, Qingdao, Shandong Province. The wheat was harvested using a combine harvester. The main impurity categories included wheat bran, straw, and spikes, which are the most common and representative types of impurities during the wheat harvesting process.

Wheat bran refers to fragments of the outer shell and germ produced during threshing. It is typically yellow or brown and has a regular shape. Straw is the residual stem of wheat plants with a smooth surface and varying thickness, appearing yellow or light yellow in color. Spikes are yellow or brown and usually consist of multiple unthreshed wheat kernels adhered together. Sample images of these impurities are shown in Figure 1.



Fig. 1 - Partial Wheat Impurity Samples

The image acquisition system used a Hikvision MV-CS060-10GC industrial camera equipped with a Hikvision MVL-HF0828-6MPE lens. The camera supported a maximum resolution of 3072×2048 pixels. During image capture, an acrylic tray was used to hold the wheat samples, and the shooting distance was fixed at 95 mm. The output image resolution was set to 2048×2048 pixels to ensure clarity and preserve the visual characteristics of the impurities. This also helped improve the precision of the subsequent labeling process. In total, 720 wheat images were collected.

The dataset was annotated using the X-AnyLabeling-GPU software and saved in YOLO format. To improve the model's generalization and robustness, the dataset was augmented through operations such as mirror flipping, 30° rotation, and brightness adjustment. A total of 2,140 images were selected for training, with the training and validation sets divided at a ratio of 8:2. The Mosaic augmentation function of YOLOv8 was also enabled during training to further enhance model robustness.

During wheat harvesting, the straw and spike impurities vary significantly in size and shape. Moreover, the relatively small sample size for these two categories makes accurate detection more difficult. While existing object detection algorithms can barely meet basic requirements, they often suffer from high complexity and large model parameters. Therefore, this study chose to improve the YOLOv8 model to better suit the task.

To enhance computational efficiency while maintaining accuracy and better utilize the computing power of the device, the Bottleneck module in the YOLOv8 C2f module was replaced with the Universal Inverted Bottleneck (UIB) module from MobileNetV4, forming a new structure named C2f\_UIB. To improve the extraction of impurity features with diverse scales and shapes, the original PANet feature fusion network was replaced by the High-level Screening Feature Pyramid Network (HS-FPN). Compared with PANet, HS-FPN achieved better multi-scale feature fusion with fewer parameters. The network structure of the improved YOLOv8 model is illustrated in Figure 2.

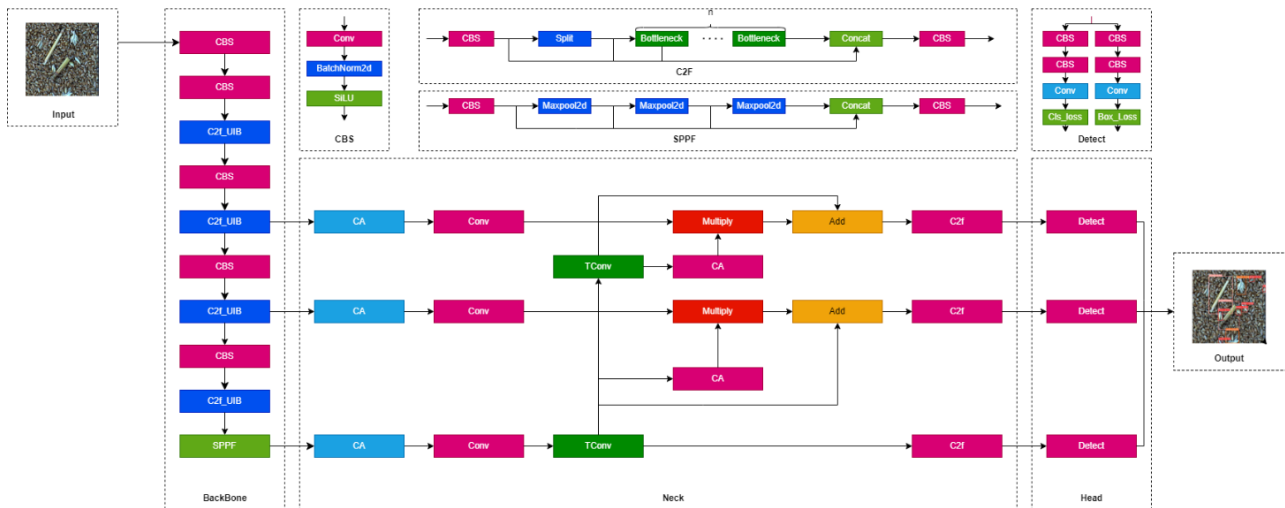


Fig. 2 - Improved YOLO v8 Lightweight Network Model

**Universal Inverted Bottleneck**

The Universal Inverted Bottleneck (UIB) was a lightweight network architecture introduced by MobileNetV4 to improve the efficiency of object detection (Qin et al., 2024). The UIB module significantly reduced the number of parameters and computational load by incorporating two optional depthwise convolutions (DW) into the Inverted Bottleneck (IB). Its core idea was to treat deep convolution as a variable structure by sharing common components such as pointwise expansion and projection. This design effectively reduced computational redundancy and optimized resource utilization efficiency.

Compared with the conventional Bottleneck structure used in the C2f module, the UIB module offered greater efficiency under limited computing resources. By replacing the Bottleneck in the C2f module with the UIB, an improved module named C2f\_UIB was constructed. Experimental results demonstrated that the new module greatly reduced computation and memory usage without sacrificing performance. This improvement was of practical significance for large-scale deep learning tasks, especially in resource-constrained environments such as edge devices or mobile applications. The application of the C2f\_UIB module further confirmed the potential and practical value of lightweight design for efficient object detection.

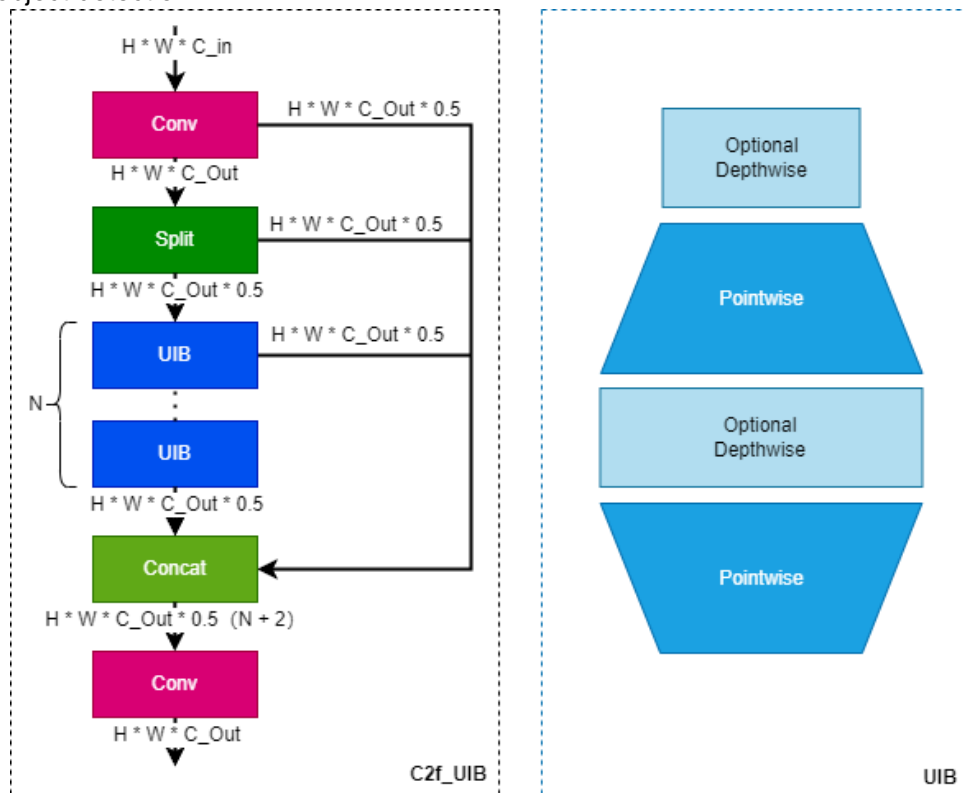


Fig. 3 - UIB Module Structure Diagram

### Feature fusion network HS-FPN

The High-level Screening Feature Pyramid Network (HS-FPN) was a multi-scale feature fusion structure designed to enhance the attention and semantic understanding capabilities of the model when detecting impurities of different sizes, particularly straw and spikes. The HS-FPN framework consisted of two major components: a feature selection module and a feature fusion module (Chen et al., 2023). These modules worked together to aggregate features of varying semantic depths and spatial resolutions, thus providing more accurate and informative representations for impurity detection. The improved HS-FPN structure adapted to the YOLOv8 backbone is shown in Figure 4.

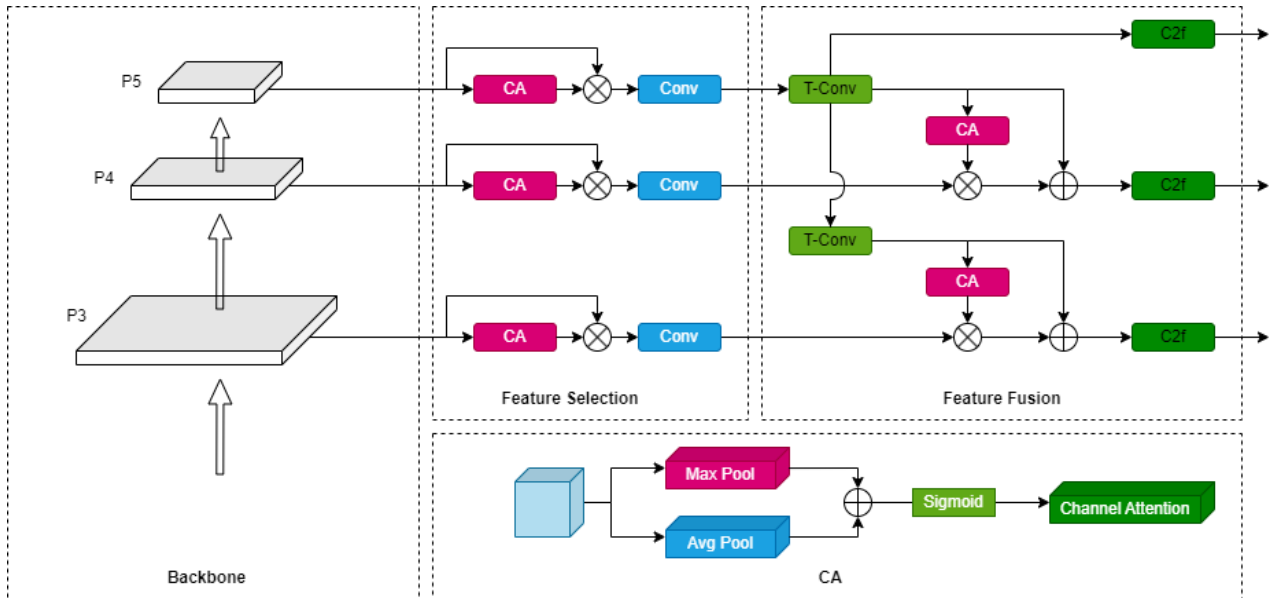


Fig. 4 – HS-FPN Structure Diagram

The feature selection module aimed to filter and reweight the multi-scale feature maps using a channel attention (CA) mechanism. As shown in the figure, the CA module first processed the input feature map using global average pooling and global max pooling to calculate the weights of each channel. These weights were then passed through a Sigmoid activation function to determine their importance. The weighted values were used to enhance the original feature map, emphasizing the most relevant feature channels for detection.

The feature fusion module served as the core component of HS-FPN. It combined feature maps of different resolutions to enhance the model's representational ability. Within this module, the Selective Feature Fusion (SFF) mechanism was used to selectively merge feature information.

The fusion process included two SFF blocks. Firstly, the high-level features with a size of  $f_{high} \in R^{C \times H \times W}$  was up sampled via transposed convolution (T-Conv) to obtain  $f_{high-T} \in R^{C \times 2H \times 2W}$  matching the scale of lower-level features. The channel attention module generated a weight vector  $f_{CA} \in R^{C \times 1 \times 1}$ , which was used to reweight the low-level feature  $f_{low}$ . The final fused feature output was calculated by the weighted addition of both:

$$f_{out} = f_{low} \times f_{CA} + f_{high-T} \quad (1)$$

This process enabled the model to leverage both detailed and abstract features. The transposed convolution and CA module jointly reconstructed the high-level features and facilitated their integration with low-level semantics. The optimization of this fusion strategy improved multi-scale feature utilization and overall detection performance.

### Optimize loss function

The original YOLOv8 model employed the Complete IoU (CIoU) loss function for bounding box regression. However, CIoU suffered from ambiguity in aspect ratio representation and was not well-suited for high-density target detection. To overcome these limitations, this study adopted the Generalized IoU (GIoU) loss, which introduced the concept of an inclusion box.

GIoU not only measured the overlap between predicted and ground truth boxes but also quantified their spatial relationship when no intersection existed, thus providing richer gradient information for optimization (Zhang *et al*, 2022).

In high-density impurity scenes, GIoU utilized the surrounding region to enhance robustness under occlusion and tight target spacing. Moreover, its simplified formulation reduced normalization overhead and lowered computational complexity. These advantages made GIoU better suited for detecting varied-scale impurities under dense distribution, offering a more stable optimization path.

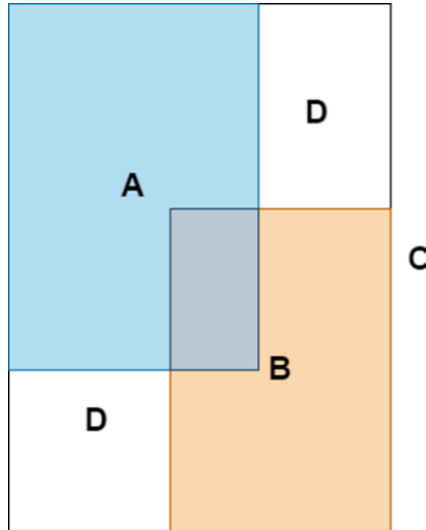


Fig. 5 – GIoU Loss Function

The GIoU is defined as:

$$GIoU = IoU - \frac{|C \setminus (A \cup B)|}{|C|} \quad (2)$$

where:  $IoU = \frac{|A \cap B|}{|A \cup B|}$ : represents the intersection and union ratio of the prediction box and the real box.  $C$ : It's the minimum closure rectangle containing the prediction box and the real box  $|C \setminus (A \cup B)|$ : It's the area in the closure rectangle that does not belong to the union of the prediction box and the real box.  $|C|$ : It's the area of the closure rectangle.

The corresponding GIoU-based loss function is:

$$L_{GIoU} = 1 - GIoU \quad (3)$$

This design not only reduced computational cost but also improved detection reliability in dense impurity scenarios.

### Indoor Experimental Setup

To evaluate the proposed impurity detection model under practical conditions, an indoor experimental system was constructed to simulate the post-harvest wheat impurity collection environment. The system consisted of a sampling box, an industrial camera (Hikvision MV-CS060-10GC), a rectangular LED light source, and a Jetson Nano embedded processor for real-time inference, as shown in Figure 6.



Fig. 6 - Structure of the indoor impurity detection system.

The camera was fixed at a certain height above the observation window to ensure clear imaging of the wheat samples. The interior of the sampling box was coated with matte material to reduce light reflection and background interference. During each test, wheat samples were spread fully across the sampling area, and the system automatically captured images under stable lighting conditions. The collected images were then processed in real time by the YOLOv8 detection model deployed on the Jetson Nano platform.

This setup replicated key aspects of a combine harvester's impurity output environment and enabled controlled validation of the model's detection accuracy. A total of 30 samples were tested in this configuration, forming the basis for performance evaluation described in the Results section.

## RESULTS

### Test environments and parameter configuration

The experimental environment is Windows10 operating system, the CPU is AMD EPYC 7402 24-Core Processor, the main frequency is 2.79 GHz, the Python 3.9.7 development environment is used, the deep learning framework is Pytorch1.12.1, the GPU uses NVIDIA GeForce RTX 3090 for computing acceleration, and the GPU runs memory of 24 GB. The software environment is configured as CUDA12.2. The input image size is 640 pixels × 640 pixels, the training rounds are set to 300 rounds, the batch size is set to 16, and the optimizer is SGD.

### Evaluating indicator

In the task of wheat impurity detection, it is essential to consider the model's accuracy, size, and deployment feasibility on edge devices. To objectively evaluate the performance of the target detection algorithms, this study employs a series of standardized evaluation metrics, including precision (P), recall (R), and mean average precision (mAP), alongside the model's memory usage and parameter count for a comprehensive performance comparison. These metrics collectively provide a thorough quantitative assessment of the model's precision, efficiency, and resource consumption in practical applications.

The calculation formula is as follows:

$$P = \frac{T_p}{T_p + F_p} \quad (4)$$

$$R = \frac{T_p}{T_p + F_n} \quad (5)$$

$$mAP = \frac{\sum_{i=1}^N AP_i}{N} \quad (6)$$

Precision measures the proportion of correctly predicted positive samples among all predicted positives, where  $T_p$  is the number of correctly detected positive samples and  $F_p$  is the number of false positives; Recall measures the proportion of actual positive samples detected by the model, where  $F_n$  is the number of missed positive samples; mean Average Precision is the average of the precision-recall curve area across all classes, with  $N$  being the total number of classes, and  $mAP$  comprehensively reflects the overall performance of the model in multi-class detection tasks.

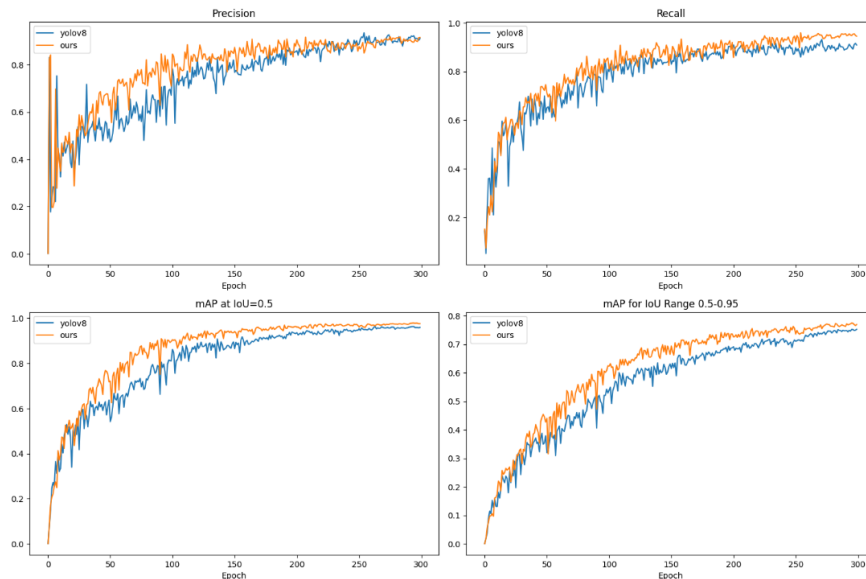
### Comparative test analysis of different algorithms

To evaluate the effectiveness of the proposed improved YOLOv8 model, it was compared with mainstream detection models, including Faster R-CNN, YOLOv5s, YOLOv7-Tiny, and the original YOLOv8n. As shown in Table 1, the improved model achieved the highest accuracy rate, recall rate, and average accuracy, outperforming all baseline models. Specifically, compared to YOLOv8n, the improved model increased accuracy by 1.0%, recall by 0.9%, and average accuracy by 1.3%. Notably, the model size was reduced by 46.7%, and parameter quantity decreased by 28.4%. This demonstrates that the lightweight design and multi-scale fusion effectively balance performance and efficiency. While YOLOv7-Tiny achieved comparable accuracy, its recall rate and average accuracy were inferior, and its parameter count remained higher. Traditional models like Faster R-CNN exhibited significantly lower performance and excessive resource consumption, highlighting the superiority of the proposed lightweight improvements.

Table 1

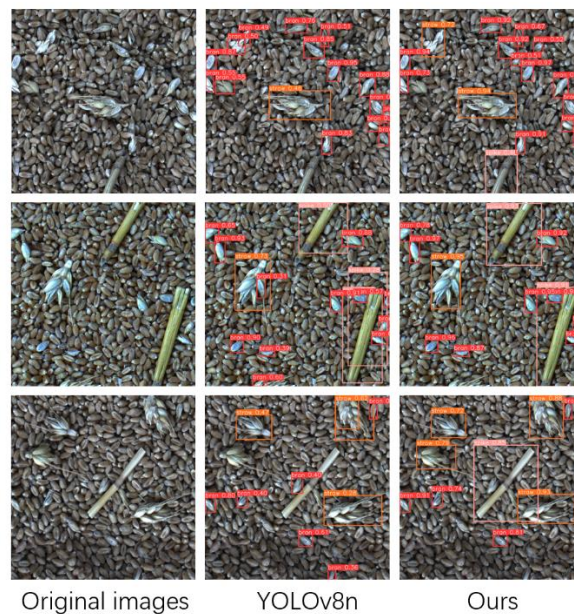
Models	Model Performance Comparison				
	accuracy rate	recall rate	average accuracy	model memory usage	parameter quantity
	[%]	[%]	[%]	[MB]	x 10 <sup>9</sup> [FLOPS]
Faster R-CNN	79.6	82.1	45.3	315.6	137.2
YOLOv5s	92.3	93.8	96.7	13.7	16.5
YOLOv7-Tiny	93.5	94.6	96.6	11.7	13.2
YOLO v8n	93.2	93.6	97.4	6.0	8.1
YOLO v8n+UIB+HSFPN+GIOU	94.2	94.5	98.7	3.2	5.8

Figure 7 shows the comparison between the improved model and YOLOv8n in terms of accuracy, recall and average accuracy. On the whole, our method performs better than YOLOv8n on all indicators.



**Fig. 7 – Performance curves of YOLOv8 model and improved YOLOv8 model**

As demonstrated in Figure 8, the enhanced YOLOv8 model exhibits superior detection performance relative to the original architecture, with notable improvements in impurity recognition capability. The optimized model achieves reduced occurrence of both missed detections and false positives, while demonstrating higher confidence scores in accurate impurity identification.



**Fig. 8 – Comparison of model detection effects**

### **Ablation test**

Ablation experiments were conducted to validate the contribution of each proposed improvement. As shown in Table 2, the baseline YOLOv8n achieved 93.2% accuracy, 93.6% recall, and 97.4% mAP. Introducing the UIB module alone slightly improved accuracy but reduced model memory usage by 11.7% and parameters by 13.6%. Replacing PANet with HS-FPN yielded more significant gains: accuracy increased to 93.7%, recall to 94.6%, and mAP to 97.8%, with a 33.3% reduction in memory. Using GloU loss alone improved recall and mAP without affecting model size. Combining UIB+HSFPN achieved 93.8% accuracy, 94.4% recall, and 98.3% mAP, while reducing memory to 3.2 MB. Finally, integrating all three improvements achieved optimal performance: 94.2% accuracy, 94.5% recall, and 98.7% mAP, confirming the synergistic effect of lightweight design, multi-scale fusion, and loss optimization.

Table 2

Models	Ablation experiment				
	Accuracy rate	Recall rate	Average accuracy	Model memory usage	Parameter quantity
	[%]	[%]	[%]	[MB]	x 10 <sup>9</sup> [FLOPS]
YOLOv8n	93.2	93.6	97.4	6.0	8.1
YOLOv8n+UIB	93.4	93.5	97.4	5.3	7.0
YOLOv8n+HSFPN	93.7	94.6	97.8	4.0	6.9
YOLOv8n+GIoU	93.6	94.3	97.7	6.0	8.1
YOLOv8n+UIB+HSFPN	93.8	94.4	98.3	3.2	5.8
YOLOv8n+UIB+HSFPN+GIoU	94.2	94.5	98.7	3.2	5.8

### Indoor Test and Validation

To evaluate the practical performance of the proposed wheat impurity detection algorithm, an indoor test was conducted under simulated harvesting conditions. The experimental setup was described in detail in the Materials and Methods section.

A total of 30 wheat samples were tested. For each sample, the system automatically captured images and detected three impurity types: wheat spike, bran, and straw. The recognition results were displayed in real-time and recorded for statistical analysis. Figure 9 shows the indoor test platform, and Figure 10 presents representative detection results.

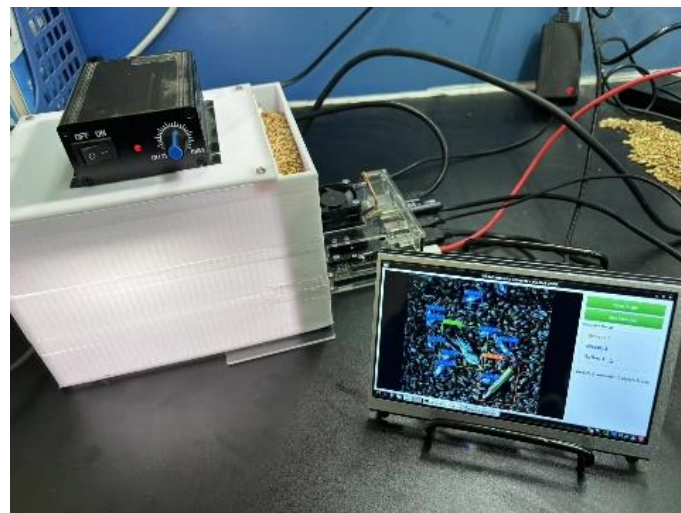


Fig. 9 – The indoor test

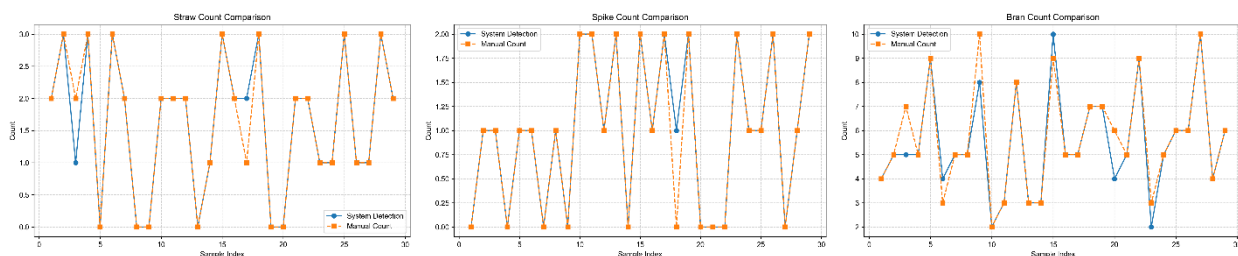


Fig. 10 – Comparison of impurity counts for systematic detection and manual annotation

According to the statistics, the model achieved high detection consistency. Only one sample had a single-object deviation in spike detection, and two samples had minor deviations in straw detection. Among the 162 bran targets, only six samples showed a one-object difference. These results validate the model's detection accuracy and robustness under realistic lighting and target distribution conditions.

The experimental outcomes further demonstrate the model's deployment potential in embedded platforms for intelligent agricultural equipment.

## CONCLUSIONS

This study proposed an improved YOLOv8-based wheat impurity detection algorithm, focusing on lightweight design, multi-scale feature fusion, and enhanced loss function. By integrating the Universal Inverted Bottleneck (C2f\_UIB), High-level Screening Feature Pyramid Network (HS-FPN), and GloU loss, the model achieved a significant reduction in computational cost while maintaining high detection accuracy.

The detection system was deployed on a Jetson Nano embedded platform and validated through indoor experiments simulating post-harvest impurity collection conditions. The experimental results demonstrated high recognition consistency and robustness, with most impurity categories exhibiting only minimal detection deviation.

Compared with existing mainstream detection models, the proposed approach offers a balanced trade-off between accuracy and efficiency, making it well-suited for real-time deployment in intelligent agricultural machinery. This work provides a practical reference for the application of deep learning in grain impurity detection, and lays a foundation for future field experiments and system integration.

## ACKNOWLEDGEMENT

The author has been supported by the “National Natural Science Foundation of China” (No.32071911), the “National Key R&D Program of China” (No.2023YFD2000404), the “Shandong Province Modern Agricultural Industry Technology System Wheat Innovation Team” (No.SDIT-0-12).

## REFERENCES

- [1] Chen, J., Lian, Y., & Li, Y. (2020). Real-time grain impurity sensing for rice combine harvesters using image processing and decision-tree algorithm. *Computers and Electronics in Agriculture*, 175, 105591.
- [2] Chen, J., Kao, S. H., He, H., Zhuo, W., Wen, S., Lee, C. H., & Chan, S. H. G. (2023). Run, don't walk: chasing higher FLOPS for faster neural networks. *Proceedings of the IEEE/CVF conference on computer vision and pattern recognition* pp. 12021-12031.
- [3] Chen, Y., Zhang, C., Chen, B., Huang, Y., Sun, Y., Wang, C., ... & Gao, Y. (2024). Accurate leukocyte detection based on deformable-DETR and multi-level feature fusion for aiding diagnosis of blood diseases. *Computers in biology and medicine*, 170, 107917.
- [4] Jia, Z., Zhang, M., Yuan, C., Liu, Q., Liu, H., Qiu, X., ... & Shi, J. (2024). ADL-YOLOv8: A Field Crop Weed Detection Model Based on Improved YOLOv8. *Agronomy*, 14(10), 2355.
- [5] Jiang, K., Xie, T., Yan, R., Wen, X., Li, D., Jiang, H., ... & Wang, J. (2022). An attention mechanism-improved YOLOv7 object detection algorithm for hemp duck count estimation. *Agriculture*, 12(10).
- [6] Li, G., Ge, H., Jiang, Y., Zhang, Y., Jiang, M., Wen, X., & Sun, Q. (2025). Research on wheat impurity identification method based on terahertz imaging technology. *Spectrochimica Acta Part A: Molecular and Biomolecular Spectroscopy*, 326, 125205.
- [7] Li, M., Zhang, Z., Lei, L., Wang, X., & Guo, X. (2020). Agricultural greenhouses detection in high-resolution satellite images based on convolutional neural networks: Comparison of faster R-CNN, YOLO v3 and SSD. *Sensors*, 20(17).
- [8] Li, P., & Zhu, C. (2024). Ro-YOLOv5: One new detector for Impurity in wheat based on Circular Smooth Label. *Crop Protection*, 184, 106806.
- [9] Liu, Q., Liu, W., Liu, Y., Zhe, T., Ding, B., & Liang, Z. (2023). Rice grains and grain impurity segmentation method based on a deep learning algorithm-NAM-EfficientNetv2. *Computers and Electronics in Agriculture*, 209, 107824.
- [10] Marjanović, M., Krautblatter, M., Abolmasov, B., Đurić, U., Sandić, C., & Nikolić, V. (2018). The rainfall-induced landsliding in Western Serbia: A temporal prediction approach using Decision Tree technique. *Engineering Geology*, 232, pp. 147-159.
- [11] Mathew, M. P., & Mahesh, T. Y. (2022). Leaf-based disease detection in bell pepper plant using YOLO v5. *Signal, Image and Video Processing*, pp. 1-7.
- [12] Mavridou, E., Vrochidou, E., Papakostas, G. A., Pachidis, T., & Kaburlasos, V. G. (2019). Machine vision systems in precision agriculture for crop farming. *Journal of Imaging*, 5(12), pp. 89.
- [13] Ok, A. O., Akar, O., & Gungor, O. (2012). Evaluation of random forest method for agricultural crop classification. *European Journal of Remote Sensing*, 45(1), pp. 421-432.

- [14] Patel, K. K., Kar, A., Jha, S. N., & Khan, M. A. (2012). Machine vision system: a tool for quality inspection of food and agricultural products. *Journal of food science and technology*, 49, pp. 123-141.
- [15] Qi, F., Wang, Y., Tang, Z., & Chen, S. (2023). Real-time and effective detection of agricultural pest using an improved YOLOv5 network. *Journal of Real-Time Image Processing*, 20(2), 33.
- [16] Qin, D., Leichner, C., Delakis, M., Fornoni, M., Luo, S., Yang, F., ... & Howard, A. (2024, September). MobileNetV4: universal models for the mobile ecosystem. In *European Conference on Computer Vision* pp. 78-96. Springer Nature Switzerland.
- [17] Redmon, J., Divvala, S., Girshick, R., & Farhadi, A. (2016). You only look once: Unified, real-time object detection. In *Proceedings of the IEEE conference on computer vision and pattern recognition*. pp. 779-788.
- [18] Ren, S., He, K., Girshick, R., & Sun, J. (2015). Faster R-CNN: Towards real-time object detection with region proposal networks. *Advances in neural information processing systems*, pp. 28.
- [19] Rezatofghi, H., Tsoi, N., Gwak, J., Sadeghian, A., Reid, I., & Savarese, S. (2019). Generalized intersection over union: A metric and a loss for bounding box regression. *Proceedings of the IEEE/CVF conference on computer vision and pattern recognition* pp. 658-666.
- [20] Shen, Y., Yin, Y., Zhao, C., Li, B., Wang, J., Li, G., & Zhang, Z. (2019). Image recognition method based on an improved convolutional neural network to detect impurities in wheat. *IEEE access*, 7, 162206-162218.
- [21] Shi, J., Bai, Y., Zhou, J., & Zhang, B. Multi-crop navigation line extraction based on improved YOLO-v8 and threshold-DBSCAN under complex agricultural environments. *Agriculture*. 2023; 14 (1): 45.
- [22] Wang, Z., Jin, L., Wang, S., & Xu, H. (2022). Apple stem/calyx real-time recognition using YOLO-v5 algorithm for fruit automatic loading system. *Postharvest Biology and Technology*, 185.
- [23] Zhang, J., Yang, W., Lu, Z., & Chen, D. (2024). HR-YOLOv8: a crop growth status object detection method based on YOLOv8. *Electronics*, 13(9), pp. 16-20.
- [24] Zhang, Y. F., Ren, W., Zhang, Z., Jia, Z., Wang, L., & Tan, T. (2022). Focal and efficient IOU loss for accurate bounding box regression. *Neurocomputing*, 506, pp. 146-157.
- [25] Zheng, Z., Wang, P., Ren, D., Liu, W., Ye, R., Hu, Q., & Zuo, W. (2021). Enhancing geometric factors in model learning and inference for object detection and instance segmentation. *IEEE transactions on cybernetics*, 52(8), pp. 8574-8586.